Hindawi
Computational Intelligence and Neuroscience
Volume 2022, Article ID 7155628, 14 pages
https://doi.org/10.1155/2022/7155628

Research Article

Nonlinear Dynamic Analysis of Bistable Piezoelectric Energy Harvester with a New-Type Dynamic Amplifier

Dawei Man,[1,2] **Gaozheng Xu**,[1] **Huaiming Xu**,[1] **Deheng Xu**,[1] **and Liping Tang**[1,2]

[1]*School of Civil Engineering, Anhui Jianzhu University, Hefei 230601, China*
[2]*BIM Engineering Center of Anhui Province, Hefei 230601, China*

Correspondence should be addressed to Dawei Man; mandawei@ahjzu.edu.cn

Received 5 May 2022; Revised 1 June 2022; Accepted 6 June 2022; Published 25 June 2022

Academic Editor: Aboul Ella Hassanien

A distributed parametric mathematical model of a new-type dynamic magnifier for a bistable cantilever piezoelectric energy harvester is proposed by using the generalized Hamilton principle. The new-type dynamic magnifier consists of a two-spring-mass system, one is placed between the fixed end of the piezoelectric beam and the L-shaped frame, and the other is placed between the L-shaped frame and the base structure. We used the harmonic balance method to obtain the analytical expressions for the steady-state displacement, steady-state output voltage, and power amplitude of the system. The effect of the distance between the magnets, the spring stiffness ratio and mass ratio of the two dynamic magnifiers, and the load resistance on the performance of the harvester is investigated. Analytical results show that compared with the bistable piezoelectric energy harvester with a typical spring-mass dynamic magnifier, the proposed new-type energy harvester system with a two-spring-mass dynamic magnifier can provide higher output power over a broader frequency band, and increasing the mass ratio of the magnifier tip mass to the tip magnet can significantly increase the output power of the BPEH + TDM system. Properly choosing the stiffness ratio of the two dynamic amplifiers can obviously improve the harvested power of the piezoelectric energy harvester at a low excitation level.

1. Introduction

In recent years, the rapid development of wireless sensor networks in building structure health and environmental monitoring has put forward higher requirements for the sustainability of its power supply. Piezoelectric energy harvesting technology is one of the most commonly used energy harvesting technologies, which collects vibration energy from the surrounding environment and converts it into useable energy [1, 2]. In the early stages, different types of linear resonant piezoelectric energy harvesters were designed to generate electrical energy from ambient vibrations. The electro-mechanical coupling equation of a linear cantilever piezoelectric energy harvester was derived and experimentally validated by Erturk and Inman [3, 4]. The ambient vibration excitation frequency usually has the characteristics of time-varying and broadband, so if the ambient vibration frequency does not match the harvester's resonant frequency, the efficiency of the linear piezoelectric energy harvester is not high [5–9]. This makes it difficult to meet the requirements of the practical application for this linear piezoelectric energy harvester [10].

The nonlinear techniques enable piezoelectric energy harvesters to achieve energy harvesting in a wider frequency band. Due to the increase of the working frequency bandwidth, the nonlinear piezoelectric energy harvester is less sensitive to the change of the external excitation frequency than the linear piezoelectric energy harvester and is more suitable for harvesting energy from the ambient vibration in practical applications [11–14]. The nonlinearity of piezoelectric energy harvesters induced by magnetic forces is usually classified into three main categories, namely, monostable [15, 16], bistable [17, 18], and tristable [19, 20]. Bistable piezoelectric energy harvesters (2 stable and 1 unstable equilibrium positions) have been extensively investigated and their broadband advantages over linear energy harvesters have been verified in simulations and experiments [21, 22]. Stanton et al. [23] established an

analytical model of a bistable piezoelectric energy harvester consisting of a permanent magnet and a piezoelectric cantilever beam and investigated the dynamic characteristics of the system using numerical simulations and experimental methods. Stanton et al. [24] studied the voltage output of a bistable cantilever piezoelectric energy harvester system under different excitation intensity and analyzed the influence of magnet spacing on the system response. He and Daqaq [25] investigated the influence mechanism of asymmetric potential well characteristics on bistable piezoelectric energy harvester under white noise excitation. Kim et al. [26] proposed an electro-mechanical coupling equation for a hysteresis reversible magneto-elastic piezoelectric energy harvester, and the analytical solutions of the system response are obtained by the multiscale method and the high-dimensional harmonic balance method, respectively. The operating bandwidth and output power of the bistable piezoelectric energy harvester have been substantially increased after entering the interwell motion. However, it requires higher excitation strength. If the excitation strength is low, the bistable energy harvester may exhibit intrawell motion which greatly reduces the output performance of the system [27].

To improve the output performance of the bistable energy harvester under low-level excitation, researchers try to make it easier to oscillate with large amplitude interwell motion. Sebald et al. [28, 29] found that external intervention and increasing the excitation amplitude can help the bistable energy harvester jump from intrawell motion to large amplitude interwell motion. However, the excitation level of the vibration in the real environment is low, and it is difficult to enter the large-scale interwell movement [30]. Ma et al. [31] proposed an asymmetric tristable energy harvester, which has a shallower and wider potential well, so that it can extract vibration energy in a wider frequency range, even at a relatively low excitation level, but the interwell output power amplitude is low in this case. Wang et al. [32] propose a configuration that includes an elastic amplifier to amplify the base excitation and provide enough kinetic energy to overcome the tristable potential well barriers, thus leading to large amplitude bistable intermotion. They only consider to amplify the vibration displacement of the base but do not consider how to further amplify the vibration amplitude of the cantilever beam. In order to further improve the performance of the energy capture device under weak excitation, a new-type bistable piezoelectric cantilever energy harvester (BPEH) with two dynamic magnifiers (TDMs) is proposed in this paper. It can amplify the amplitude of the low-level base excitation and the vibration amplitude of the fixed end of the piezoelectric cantilever beam at the same time, so as to dramatically improve the output power and effective bandwidth of the piezoelectric energy harvester. Considering the size effect of the tip magnet, the distributed parameter electro-mechanical coupling equation of the bistable piezoelectric energy harvester with two dynamic magnifiers (BPEH + TDM) is established based on the generalized Hamilton principle, and the analytical solution of the energy capture system is derived by using the harmonic balance method. The effects of the distance between the magnets, the mass of the dynamic magnifiers, the load resistance, and the stiffness ratio of the two dynamic magnifiers on the performance of the energy capture system were studied. The results show that compared with the typical bistable piezoelectric energy harvester with a dynamic magnifier, the piezoelectric proposed energy harvester system with a two-spring-mass dynamic magnifier can collect higher output power over a broader frequency band. By reasonably selecting the design parameters of the amplifier, the harvested power can be significantly increased and the effective bandwidth of the harvester can be improved. The mathematical model of the BPEH + TDM is described in Section 2. The harmonic balance method is used for analytical expressions for the steady-state displacement, steady-state output voltage, and power amplitude of the BPEH + TDM in Section 3. The effects of parameter variations of the BPEH + TDM on its dynamic characteristics are numerically investigated in Section 4.

2. Mathematical Model of the BPEH + TDM

The BPEH + TDM configuration considered in this paper is schematically shown in Figure 1. The BPEH comprises a piezoelectric cantilever beam and two magnets (denoted as A and B). The piezoelectric cantilever beam is composed of a substrate layer, covered with a pair of piezoelectric layers (PZTs) on both of its surfaces, and poled oppositely in the thickness direction. The two piezoelectric layers are electrically connected in series with a load resistance (R), representing the equivalent resistance of a low power electronic device. Magnet A (called the tip magnet) is attached to the tip of the cantilever beam and the external magnet B is fixed at the right wall of the L-shaped frame. The TDM comprises two dynamic magnifiers (denoted as DM1 and DM2), the DM1 is basically a spring (k_{f})-mass (M_{f}) system placed between the fixed end of the piezoelectric beam and the bottom of the L-shaped frame, and the DM2 composed an L-shaped frame and a spring k_{b}, and the L-shaped frame is mechanically connected in series with the spring k_{b}. M_{f} and M_{m} represent the mass of DM1 and DM2, respectively. The horizontal gap between the tip magnet and magnet B is d. Here, l and b are the length and width of the piezoelectric cantilever beam, respectively; h_{s} and t_{p} denote the thickness of the substrate layer and the PZTs, respectively; e is the eccentricity of the tip magnet.

$v_m(t)$ and $v_b(t)$ represent the vibration displacement of the DM2 and the base, respectively. s is the coordinate along the neutral axis of the beam, and $v(s, t)$ represents the displacement of the beam at s position relative to its fixed end. The constitutive equations of the piezoelectric cantilever beam are assumed as follows:

$$\left.\begin{aligned} T_1^s &= Y_s S_1^s \\ T_1^p &= Y_p\left(S_1^p - d_{31}E_3\right) \\ D_3 &= d_{31}T_1 + \varepsilon_{33}^T E_3 \end{aligned}\right\}. \tag{1}$$

Here, Y is Young's modulus, subscript/superscript p and s represent the piezoelectric layers and substrate layer, and S_1

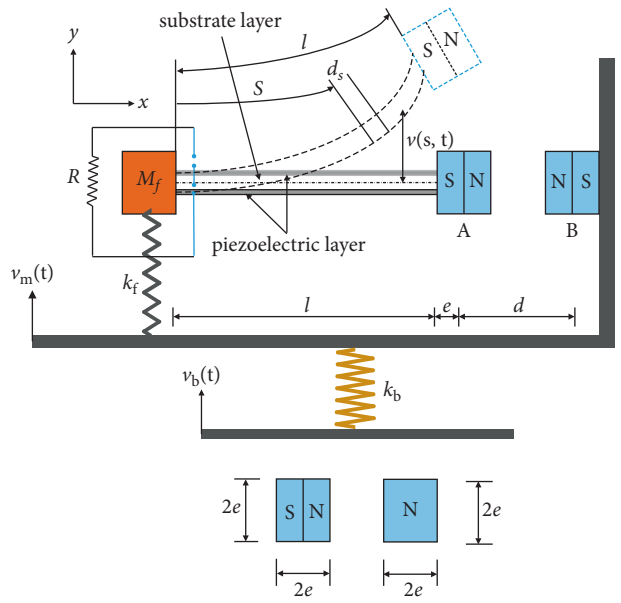

FIGURE 1: Schematic of the considered BPEH + TDM.

and T_1 are the strain and the stress of the beam, respectively. D_3 is the electric displacement and d_{31} and ε_{33}^T are the piezoelectric constant and dielectric constant, respectively. $E_3 = -V(t)/(2t_P)$ is the electric field, in which $V(t)$ represents the voltage. The strain generated in the piezoelectric beam can be assumed as $S_1^s = S_1^p = -yv''$.

The generalized Hamilton's principle of the BPEH + TDM system is as follows:

$$\int_{t_1}^{t_2} \left[\delta\left(T_{\mathrm{k}} + W_e - U_{\mathrm{e}} - U_{\mathrm{m}} - U_{\mathrm{d}}\right) + \delta W\right]\mathrm{d}t = 0. \tag{2}$$

Here, T_{k}, W_{e}, U_{e}, U_{m}, U_{d}, and W are the kinetic energy, the electrical energy, the strain energy, the magnetic potential energy, the elastic potential of the dynamic magnifiers, and the external work, respectively. T_{k} and W_{e} are as follows:

$$\begin{aligned} T_k = {} & \frac{1}{2}\int_0^l m\left(\dot{v} + \dot{v}_m(t)\right)^2 \mathrm{d}s + \frac{1}{2}M_t\left(\dot{v}(l,t) + e\dot{v}'(l,t) + \dot{v}_m(t)\right)^2 + \frac{1}{2}J\dot{v}'(l,t)^2 \\ & + \frac{1}{2}M_f\left(\dot{v}(0,t) + \dot{v}_m(t)\right)^2 + \frac{1}{2}M_m\dot{v}_m(t)^2, \end{aligned} \tag{3}$$

$$W_e = \frac{1}{2}Y_p b d_{31}\left(h + \frac{t_p}{2}\right)V(t)\int_0^l v''\mathrm{d}s + bl\varepsilon_{33}^S\frac{V(t)^2}{4t_p}. \tag{4}$$

Here, $m = 2\rho_p t_p b + \rho_s h_s b$, in which ρ_p and ρ_s are the density of the piezoelectric layers and substrate layer, respectively. M_{t} is the tip magnet mass and J represents the rotary inertia of the tip magnet, ε_{33}^s is the permittivity.

U_{e} is expressed as follows:

$$U_{\mathrm{e}} = \frac{1}{2}\int_0^l \left[YIv''^2 - Y_{\mathrm{p}} b d_{31}\left(h + \frac{t_{\mathrm{p}}}{2}\right)V(t)v''\right]\mathrm{d}s. \tag{5}$$

Here, $h = (h_s/2)$, $YI = (2/3)[Y_s b h^3 + Y_p b(3h^2 t_p + 3ht_p^2 + t_p^3)]$.

U_{d} is expressed as follows:

$$U_d = \frac{1}{2}k_f v(0,t)^2 + \frac{1}{2}k_b v_m^2. \tag{6}$$

Here, k_{f} and k_{b} represent the stiffness of DM1 and DM2, respectively. Considering the eccentricity of the tip magnet, U_{m} can be given by the following equation:

$$U_{\mathrm{m}} = \mu_0 M_{\mathrm{A}} V_{\mathrm{A}} M_{\mathrm{B}} V_{\mathrm{B}} \left\{ -\left(v(l,t) + \frac{ev'(l,t)}{\sqrt{1+v'(l,t)^2}} \right)^2 + 2\left[d + e\left(1 - \frac{1}{\sqrt{1+v'(l,t)^2}} \right) \right]^2 \right.$$
$$\left. -3\left[d + e\left(1 - \frac{1}{\sqrt{1+v'(l,t)^2}} \right) \right] \left(v(l,t) + \frac{ev'(\mathrm{l},\mathrm{t})}{\sqrt{1+v'(l,t)^2}} \right) v'(l,t) \right\} \tag{7}$$
$$4\pi \sqrt{1+v'(l,t)^2} \left\{ \left[d + e\left(1 - \frac{1}{\sqrt{1+v'(l,t)^2}} \right) \right]^2 + \left(v(l,t) + \frac{ev'(l,t)}{\sqrt{1+v'(l,t)^2}} \right)^2 \right\}^{5/2}.$$

Here, $\mu_0 = 4\pi \times 10^{-7} H \cdot m^{-1}$ is the magnetic permeability constant. M_{A} (M_{B}) and V_{A} (V_{B}) are the magnetization intensity and volume of the magnet A (B), respectively.

Using the Galerkin approach, $v(s,t)$ can be written as follows:

$$v(s,t) = \phi_r(s)\eta_r(t). \tag{8}$$

Here, $\varphi_r(s)$ and $\eta_r(t)$ represent the R-order mode shape function and the generalized mode coordinates of the beam, respectively.

The modal shape function satisfies the following orthogonal relations:

$$\int_0^l \phi_s(s) m \phi_r(s) \mathrm{d}s + \phi_s(l) M_t \phi_r(l) + \phi_s(l) M_t e \phi_r'(l) + \phi_s(0) M_f \phi_r(0)$$
$$+ \phi_s'(l)\left(J + M_t e^2\right)\phi_r'(l) + \phi_s'(l) M_t e \phi_r(l) = \delta_{rs}, \tag{9}$$

$$\int_0^l \frac{\mathrm{d}^2\phi_s(s)}{\mathrm{d}s^2} YI \frac{\mathrm{d}^2\phi_r(s)}{\mathrm{d}s^2} \mathrm{d}s + \phi_s(0) k_f \phi_r(0) = \omega_r^2 \delta_{rs}. \tag{10}$$

Here, δ_{rs} represents the Kronecker delta. $\omega_r = \lambda_r^2 \sqrt{YI/(ml^4)}$ represents the resonance frequency of the r-th mode, in which λ_r is the eigenvalue. The calculation process of the λ_r is described in the literature [33, 34].

Substituting equation (8) into (7), the Taylor's expansion of U_m at $\eta(t) = 0$ can be expressed as follows:

$$U_m = k_0 - \frac{1}{2} k_1 \eta_1^2 + \frac{1}{4} k_2 \eta_1^4 + o\left(\eta_1^5\right). \tag{11}$$

Here, $k_0 = 2\kappa/d^3$,

$$k_1 = \frac{\kappa\left(10q_1 + 2d^2\phi_1'(l)^2 + 2q_2\right)}{d^5},$$

$$k_2 = \frac{\kappa\left[8d^2 q_3 + 35q_1^2 + 10\left(d^2\phi_1'(l)^2 + q_2\right)q_1 + \left(3d^2\phi_1'(l)^4 + 2q_2\phi_1'(l)^2 + 4q_4\right)d^2\right]}{d^7},$$

$$q_1 = de\phi_1'(l)^2 + e^2\phi_1'(l)^2 + 2e\phi_1(l)\phi_1'(l) + \phi_1(l)^2,$$

$$q_2 = \left(e\phi_1'(l) + \phi_1(l)\right)^2 - 2\ de\ \phi_1'(l)^2 + 3\ d\left(e\phi_1'(l) + \phi_1(l)\right)\phi_1'(l),$$

$$q_3 = 2.5\left(0.75\ de\ \phi_1'(l)^4 + 0.75e^2\phi_1'(l)^4 + e\phi_1(l)\phi_1'(l)^3\right),$$

$$q_4 = \left(e\phi_1'(l) + \phi_1(l)\right)e\phi_1'(l)^3 - 1.5\ de\ \phi_1'(l)^4 + 0.5e^2\phi_1'(l)^4 - 3\left[-0.5\ de\ \phi_1'(l)^3 + 0.5e\phi_1'(l)^2\left(e\phi_1'(l) + \phi_1(l)\right)\right]\phi_1'(l),$$
$$\kappa = \frac{\mu M_A V_A M_B V_B}{4\pi}, \tag{12}$$
$$\delta W = \delta v_m \ddot{v}_b\left(M_m + M_t + ml + M_f\right) + \delta\eta(t)\ddot{v}_b\left(M_t\phi_1(l) + m\int_0^l \phi_1(s)\mathrm{d}s + M_t e\phi_1'(l) + M_f\phi_1(0)\right).$$

The external virtual work can be defined as follows.

Substituting equation (8) into (2) and considering only the 1st order mode, Lagrange's equation for the BPEH + TDM system is given by the following equation:

$$\begin{cases} \dfrac{\mathrm{d}}{\mathrm{d}t}\left(\dfrac{\partial L}{\partial \dot{v}_m}\right) - \dfrac{\partial L}{\partial v_m} + \dfrac{\partial W}{\partial v_m} = 0, \\ \dfrac{\mathrm{d}}{\mathrm{d}t}\left(\dfrac{\partial L}{\partial \dot{\eta}}\right) - \dfrac{\partial L}{\partial \eta} + \dfrac{\partial W}{\partial \eta} = F(t), \\ \dfrac{\mathrm{d}}{\mathrm{d}t}\left(\dfrac{\partial L}{\partial \dot{V}}\right) - \dfrac{\partial L}{\partial V} + \dfrac{\partial W}{\partial V} = Q(t). \end{cases} \tag{13}$$

Here, $F_1(t) = -2\xi_1\omega_1\dot{\eta}_1(t)$ is the generalized dissipative force, ξ_1 is the damping ratio, and $Q(t) = V(t)/R$ represents the generalized output charge.

The electro-mechanical coupling equations of the BPEH + TDM system can be obtained by using the following equation:

$$\begin{cases} M_0\ddot{\eta}_1(t) + M_1\ddot{v}_m(t) + k_b v_m = -M_1\ddot{v}_b(t), \\ \ddot{\eta}_1(t) + 2\xi_1\omega_1\dot{\eta}_1(t) + \omega_1^2\eta_1(t) - k_1\eta_1(t) + k_2\eta_1(t)^3 - \theta_1 V(t) + M_0\ddot{v}_m(t) = -M_0\ddot{v}_b(t), \\ C_p\dot{V}(t) + \dfrac{V(t)}{R} + \theta_1\dot{\eta}_1(t) = 0. \end{cases} \tag{14}$$

Here, $M_0 = m\int_0^l \varphi_1(s)\mathrm{d}s + M_t\varphi_1(l) + M_t e\varphi_1'(l) + M_f\varphi_1(0)$, $M_1 = ml + M_t + M_f + M_m$, $\omega_1^2 = YI\int_0^l \varphi_1''(s)^2\mathrm{d}s + k_f\varphi_1(0)^2$, $\theta_1 = Y_p bd_{31}(h + (t_p/2))\int_0^l \varphi_1''(s)\mathrm{d}s$, $C_p = bl\varepsilon_{33}^S/2t_p$. Here, $\omega_1^2 = YI\int_0^l \varphi_1^{''}\mathrm{d}s$, $g_0 = mg\int_0^l \varphi_1(s)\mathrm{d}s + M_t g\varphi_1(l)$, $\Gamma_1 = m\int_0^l \varphi_1(s)ds + M_t(\varphi_1(l) + e\varphi_1'(l))$, $\theta_1 = Y_p bd_{31}(h + (t_p/2))\int_0^l \varphi_1(s)\mathrm{d}s$, and $C_p = bl\varepsilon_{33}^S/2t_p$.

The excitation acceleration is assumed to be $\ddot{v}_b(t) = \ddot{v}_b cos(\omega_e t)$, where $\ddot{v}_b$ denotes the excitation amplitude, ω_e denotes the circular frequency, and C_p denotes the capacitance. Introducing the dimensionless parameters $x = \eta_1/l$, $V_m = v_m/l$, $V_b = v_b/l$, $\ddot{V} = (VC_p/l\theta_1)$, $\tau = \omega_1 t$, equation (14) can be rewritten as the following equation in the dimensionless form:

$$\begin{cases} \dfrac{M_1 - M_0^2}{K_b}x^{(4)} + \dfrac{2M_1\xi_1}{K_b}x^{(3)} + \dfrac{M_1(1-K_1) + K_b}{K_b}\ddot{x} + 2\xi_1\dot{x} + (1-K_1)x + K_2x^3 \\ + \dfrac{M_1K_2}{K_b}\left(6x\dot{x}^2 + 3x^2\ddot{x}\right) - \dfrac{M_1\Theta}{K_b}\ddot{V} - \Theta\ddot{V} = F\ cos(\omega\tau), \\ \ddot{V} + \alpha\ddot{V} + \dot{x} = 0. \end{cases} \tag{15}$$

Here, $K_b = k_b/\omega_1^2$, $K_1 = k_1/\omega_1^2$, $K_2 = k_2 l^2/\omega_1^2$, $\Theta = \theta_1^2/C_p\omega_1^2$, $\alpha = 1/C_p R_L \omega_1$, $F = -M_0 v_b/\omega_1^2 l$.

3. Harmonic Balance Analysis

The solution of equation (15) is assumed to be

$$\begin{cases} x = A(\tau) + B(\tau)\sin(\omega\tau) + C(\tau)\cos(\omega\tau), \\ \overline{V} = D(\tau)\sin(\omega\tau) + E(\tau)\cos(\omega\tau). \end{cases} \tag{16}$$

Here, A, B, C, D, and E are undetermined coefficients, so the displacement amplitude can be expressed as $a = \sqrt{B^2 + C^2}$ and the output voltage amplitude can be expressed as $u = \sqrt{D^2 + E^2}$.

Substituting equation (16) into (15), let the constant terms on both sides of the equation and the coefficients of $\sin(\omega\tau)$ and $\cos(\omega\tau)$ consistent and ignoring the high-order harmonic term and partial zero term, we can obtain the following equations:

$$Z_1\ddot{A} + 2\xi_1\dot{A} + (1 - K_1)A + K_2A^3 + \frac{3}{2}K_2A\left(B^2 + C^2\right) = 0, \tag{17}$$

$$Z_1(\ddot{B} - 2\omega\dot{C}) + 2\xi_1\dot{B} + Z_2C + Z_3B + Z_4D = 0, \tag{18}$$

$$Z_1(\ddot{C} - 2\omega\dot{B}) + 2\xi_1\dot{C} + Z_3C - Z_2B + Z_4E - F = 0, \tag{19}$$

$$\dot{D} - \omega E + \alpha D + \dot{B} - \omega C = 0, \tag{20}$$

$$\dot{E} + \omega D + \alpha E + \dot{C} + \omega B = 0. \tag{21}$$

Here,

$$\begin{aligned} Z_1 &= \frac{K_1M_1 + K_b}{K_b}, \\ Z_2 &= \frac{2\xi_1M_1}{K_b}\omega^3 - 2\xi_1\omega, \\ Z_3 &= \frac{M_1 - M_0^2}{K_b}\omega^4 - \frac{(1 - K_1)M_1 + K_b}{K_b}\omega^2 + 1 - K_1 + K_2\left(3A^2 + \frac{3}{4}a^2\right) - \frac{K_2M_1}{K_b}\omega^2\left(3A^2 + \frac{3}{4}a^2\right), \\ Z_4 &= \frac{\Theta M_1}{K_b}\omega^2 - \Theta. \end{aligned} \tag{22}$$

As the undetermined coefficients A, B, C, D, and E in equations (17)–(21) change slowly, it can be considered that

$$\begin{cases} \dfrac{dA}{d\tau} = \dfrac{dB}{d\tau} = \dfrac{dC}{d\tau} = \dfrac{d\,D}{d\tau} = \dfrac{dE}{d\tau} = 0, \\ \dfrac{d^2A}{d\tau^2} = \dfrac{d^2B}{d\tau^2} = \dfrac{d^2C}{d\tau^2} = \dfrac{d^2D}{d\tau^2} = \dfrac{d^2E}{d\tau^2} = 0, \\ \dfrac{d^3A}{d\tau^3} = \dfrac{d^3B}{d\tau^3} = \dfrac{d^3C}{d\tau^3} = 0, \\ \dfrac{d^4A}{d\tau^4} = \dfrac{d^4B}{d\tau^4} = \dfrac{d^4C}{d\tau^4} = 0. \end{cases} \tag{23}$$

Using equations (20) and (21), we obtain the following equations:

$$D = \frac{\omega}{\omega^2 + \alpha^2}(\alpha C - \omega B), \tag{24}$$

$$E = -\frac{\omega}{\omega^2 + \alpha^2}(\omega C + \alpha B). \tag{25}$$

Then, substituting formulas equations (20) and (21) into equations (18) and (19), respectively, we obtain the following equations:

$$B = -\frac{F\left(Z_2 + Z_4\left(\alpha\omega/\omega^2 + \alpha^2\right)\right)}{\left(Z_3 - \left(Z_4\omega^2/\left(\omega^2 + \alpha^2\right)\right)\right)^2 + \left(Z_2 + \left(Z_4\alpha\omega/\left(\omega^2 + \alpha^2\right)\right)\right)^2}, \tag{26}$$

$$C = -\frac{F\left(\left(Z_4\omega^2/\left(\omega^2 + \alpha^2\right)\right) - Z_3\right)}{\left(Z_3 - \left(Z_4\omega^2/\left(\omega^2 + \alpha^2\right)\right)\right)^2 + \left(Z_2 + \left(Z_4\alpha\omega/\left(\omega^2 + \alpha^2\right)\right)\right)^2}. \tag{27}$$

Therefore, the displacement amplitude and the voltage amplitude can be expressed as follows:

$$a^2\left[\left(Z_2 + Z_4\frac{\alpha\omega}{\omega^2 + \alpha^2}\right)^2 + \left(Z_3 - Z_4\frac{\omega^2}{\omega^2 + \alpha^2}\right)^2\right] = F^2. \tag{28}$$

Here, the steady-state displacement response amplitude a can be obtained by equation (23), and the steady-state output voltage amplitude and output power amplitude can then be expressed in the following forms:

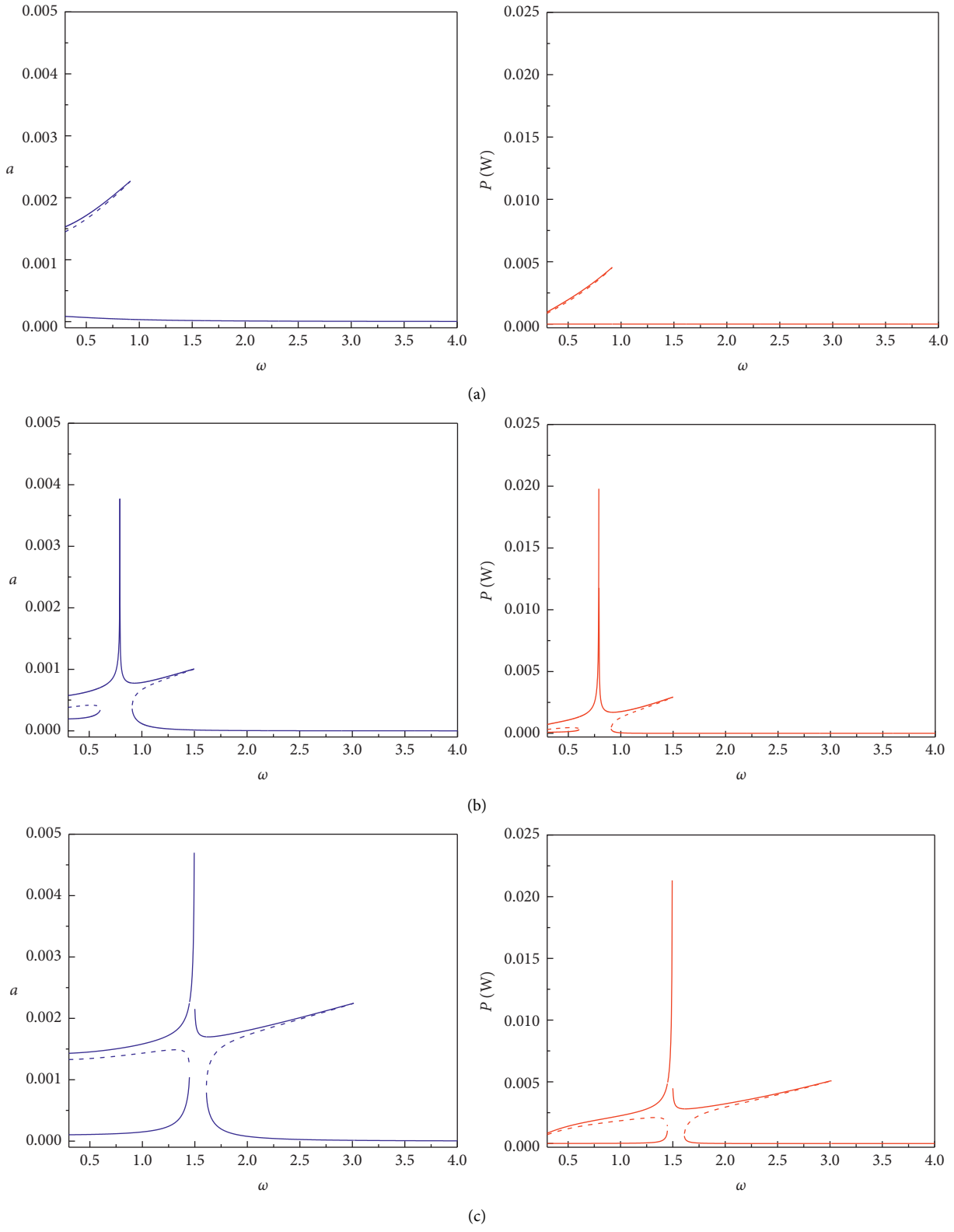

FIGURE 2: Displacement amplitude (left column) and output power amplitude (right column) versus excitation frequency for: (a) BPEH + DM1. (b) BPEH + DM2. (c) BPEH + TDM when $d = 16$ mm.

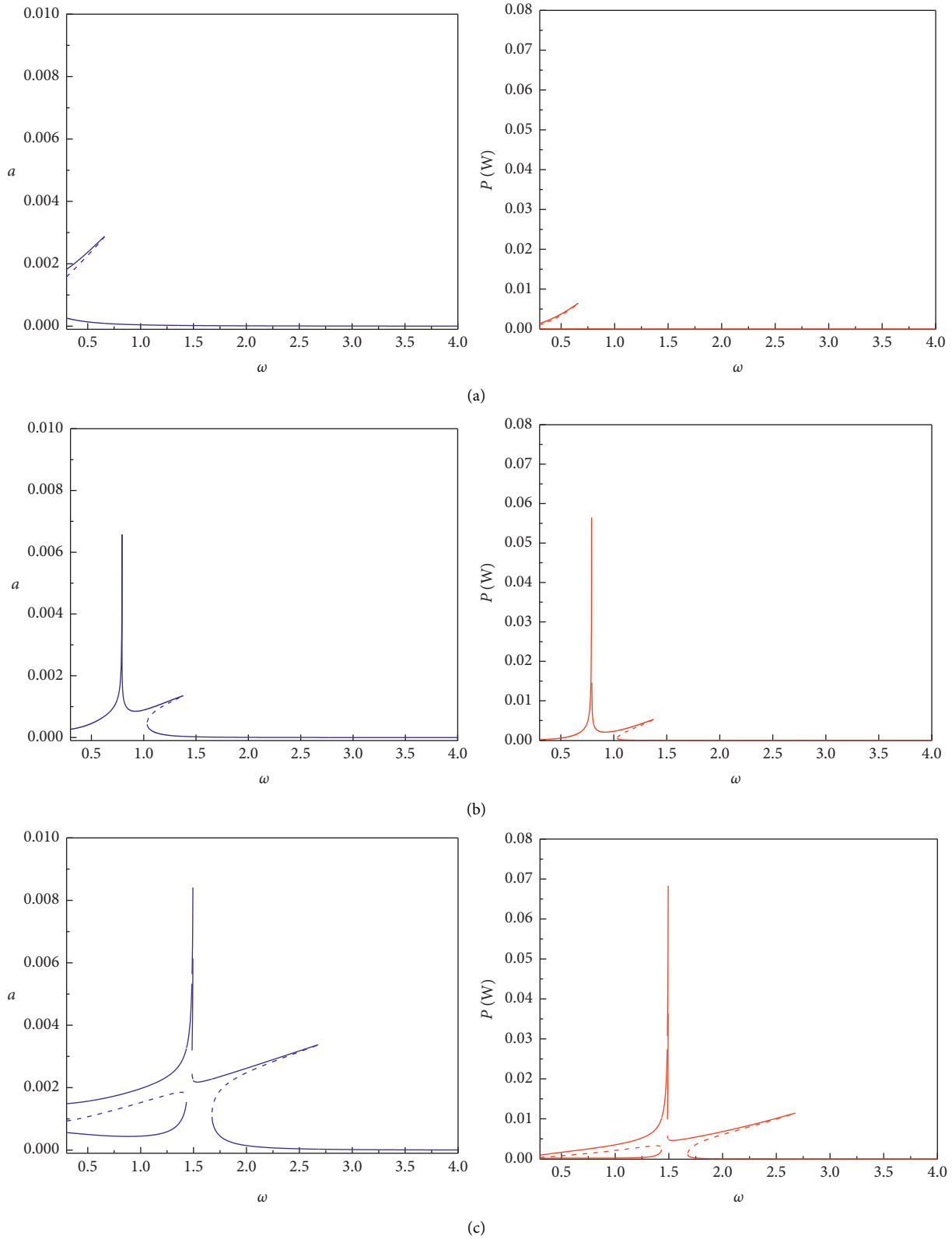

Figure 3: Displacement amplitude (left column) and output power amplitude (right column) versus excitation frequency for: (a) BPEH + DM1. (b) BPEH + DM2. (c) BPEH + TDM when $d = 20$ mm.

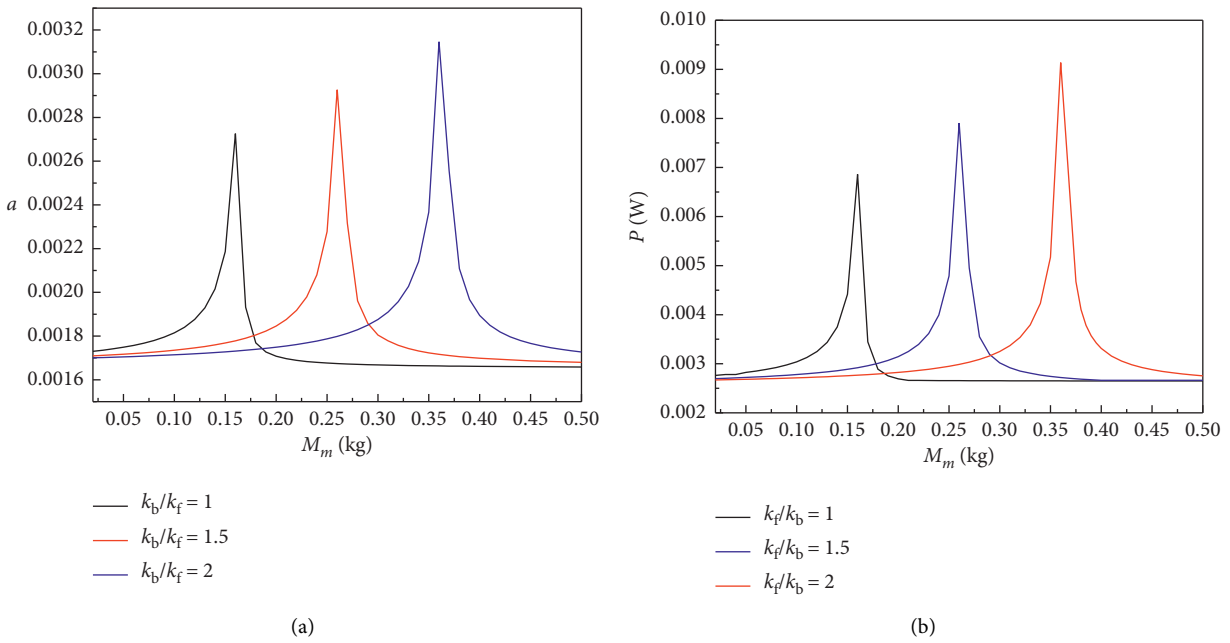

(a) (b)

Figure 4: (a) Displacement amplitude and (b) output power amplitude versus the mass of the base amplifier M_m for excited frequency $\omega = 1.4$ with different value of the stiffness ratio k_f/k_b.

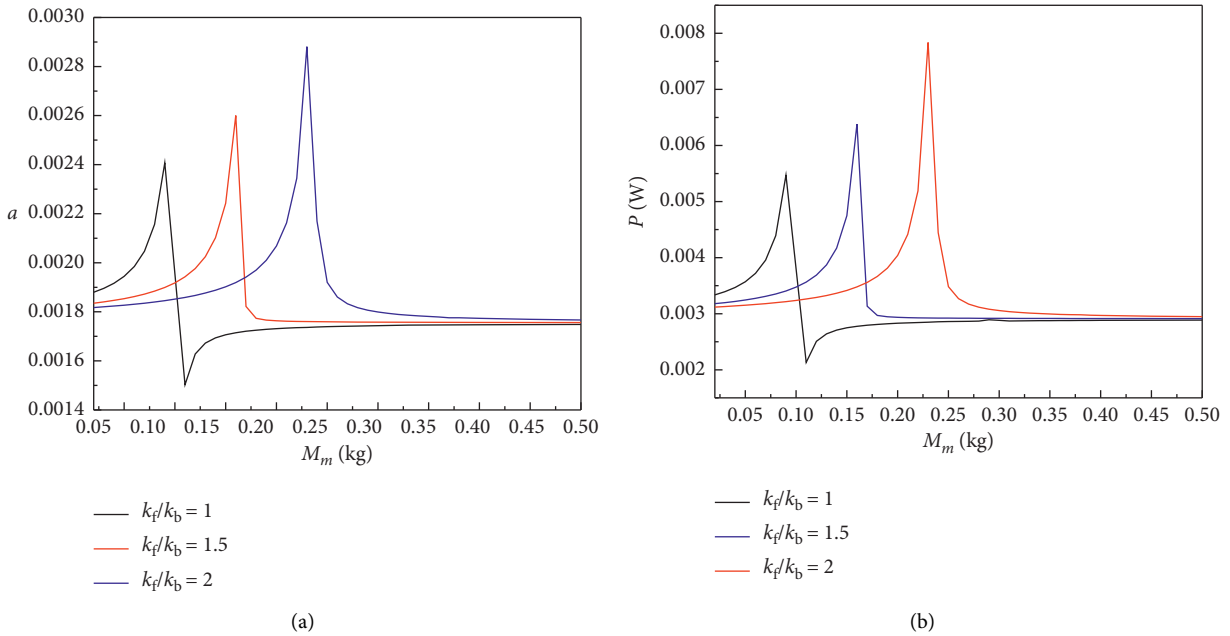

(a) (b)

Figure 5: (a) Displacement amplitude and (b) output power amplitude versus the mass of the base amplifier M_m for excited frequency $\omega = 1.7$ with different value of the stiffness ratio k_f/k_b.

$$u = \left(\frac{\omega}{\sqrt{\omega_2 + \alpha^2}} \right) a, \tag{29}$$

$$P = \frac{l^2 \theta_1^2 u^2}{C_p^2 R}. \tag{30}$$

4. Results and Discussion

In this section, we numerically investigate the effects of the magnet spacing, the mass of the base dynamic magnifier M_m, the load resistance, the stiffness ratio of the k_f to k_b, and the mass ratio of the M_f to M_t on the dynamic characteristics of the BPEH + TDM system. The geometric and material

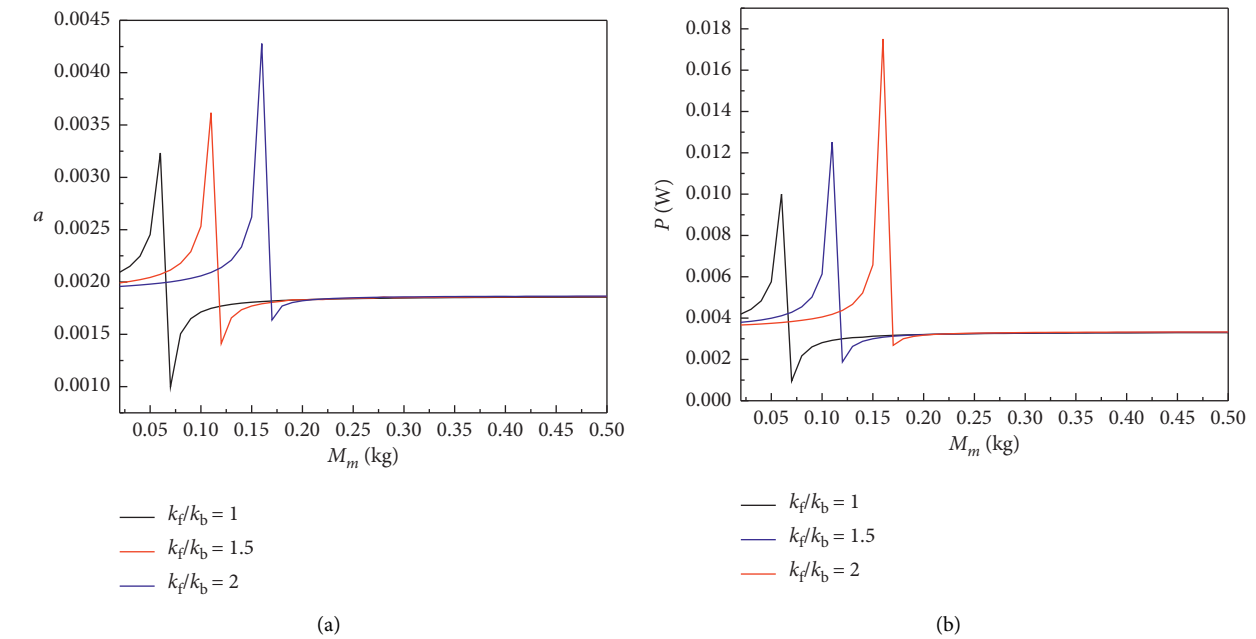

FIGURE 6: (a) Displacement amplitude and (b) output power amplitude versus the mass of the base amplifier M_m for excited frequency $\omega = 2$ with different value of the stiffness ratio k_f/k_b.

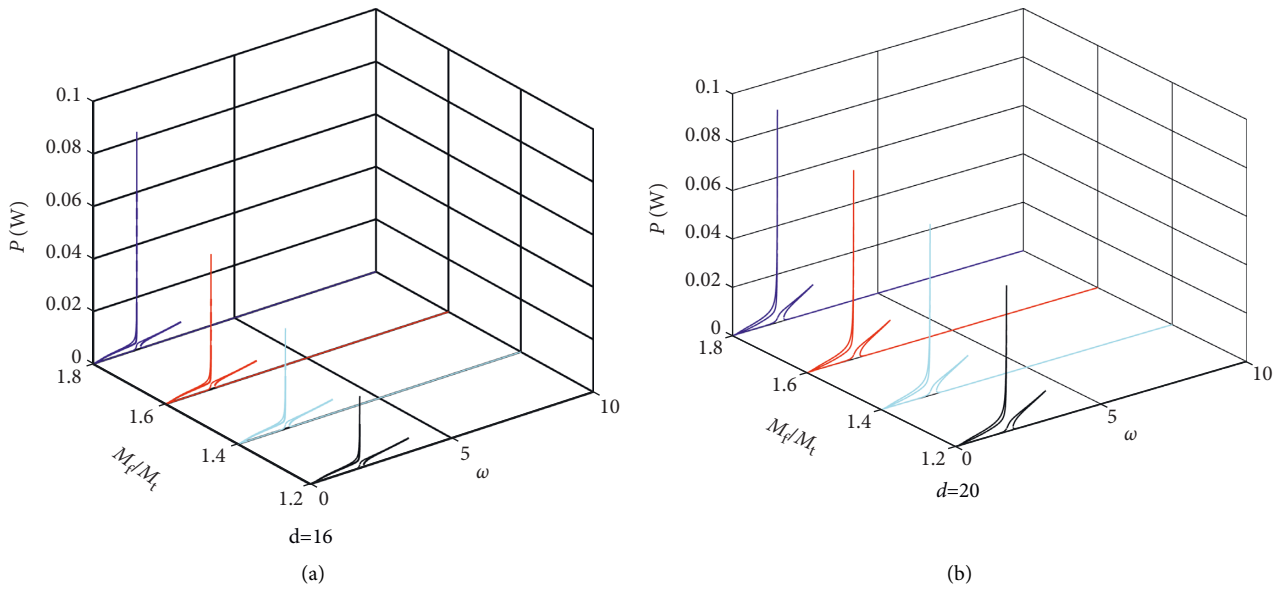

FIGURE 7: Power frequency response curve in different values of the mass ratio M_f/M_t for $M_m = 0.12$ kg when (a) $d = 16$ mm, (b) $d = 20$ mm.

properties are as follows [35]: $l = 75mm$, $b = 20mm$, $h_s = 0.2mm$, $Y_s = 70Gpa$, $\rho_s = 2700\text{kg/m}^3$, $M_t = 10\times 10^{-3}kg$, $M_m = 0.18kg$, $M_f = 16.5\times 10^{-3}kg$, $k_f = 10.2KN\cdot m$, $k_b = 15.8KN\cdot m$ $M_A = M_B = 1.22\times 10^6 A/m$, $V_A = V_B = 1\times 10^{-6}m^3$, $\xi_1 = 0.01$. $Y_p = 60.98Gpa$, $\rho_s = 7750kg/m^3$, $d_{31} = -1.71\times 10^{-10}C/N$, $\varepsilon_{33}^s = 1.33\times 10^{-8}F/m$.

In Figures 2 and 3, we define three bistable piezoelectric energy harvester (BPEH) calculation models, namely, BPEH + DM1 (BPEH with a dynamic amplifier placed between the fixed end of the piezoelectric beam and the base structure), BPEH + DM2 (BPEH with a dynamic amplifier placed between the BPEH and the base structure), and BPEH + TDM (BPEH with DM1 and DM2 amplifiers). Figure 2 depicts variations of displacement and output power versus excited frequency for different calculation models when $d = 16$ mm, $M_t = 10$ g, $M_f = 16.5$ g, and $R = 300$ kΩ. It shows that among the three calculation models, the peak displacement and peak power of the interwell motion of BPEH + TDM are the highest, and its frequency bandwidth is also the widest. When magnet spacing d increases to 20 mm, it can be seen from Figure 3

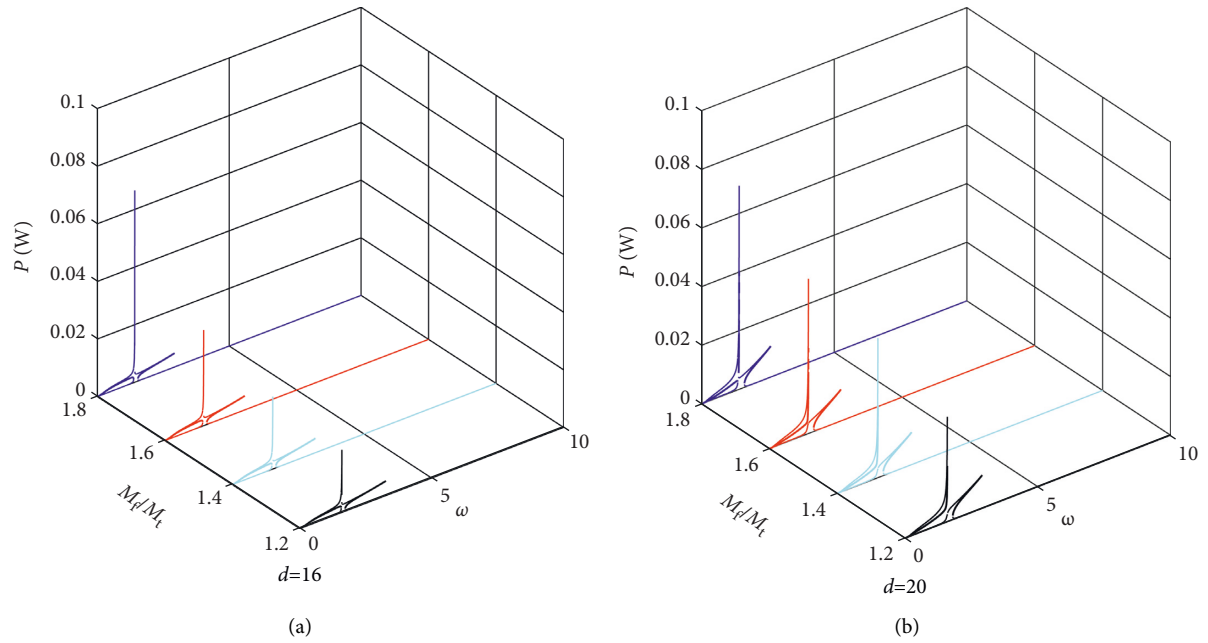

Figure 8: Power frequency response curve in different values of the mass ratio M_f/M_t for $M_m = 0.15$ kg when (a) $d = 16$ mm, (b) $d = 20$ mm.

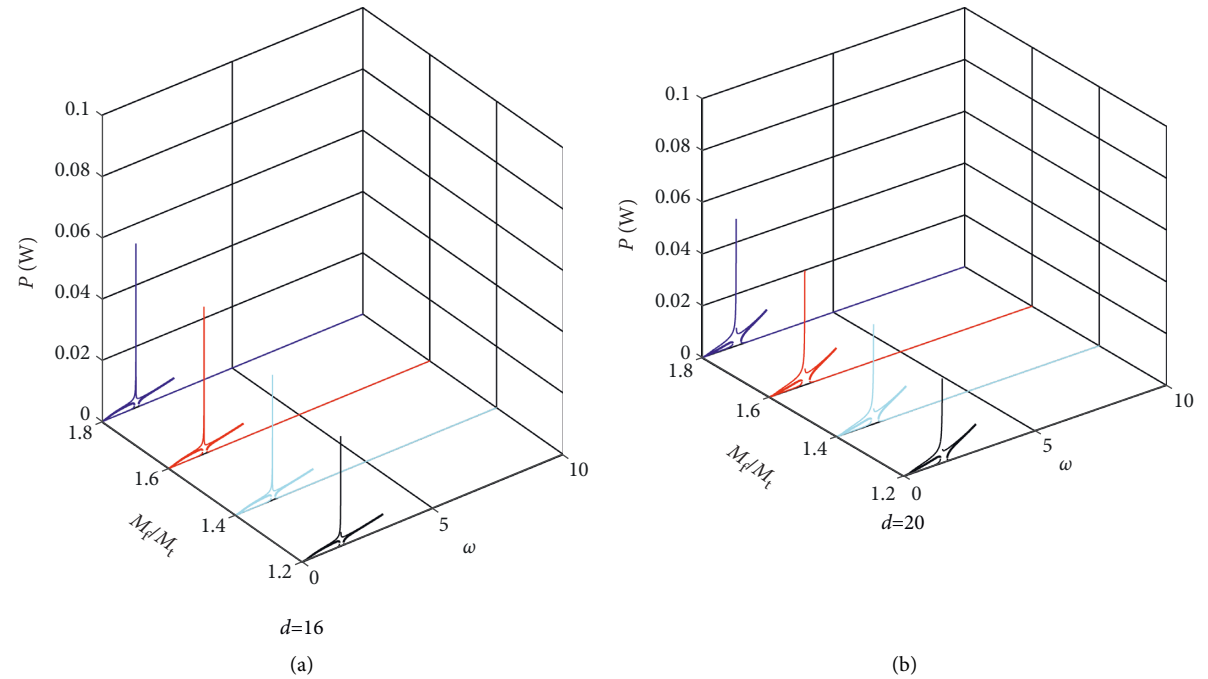

Figure 9: Power frequency response curve in different values of the mass ratio M_f/M_t for $M_m = 0.18$ kg when (a) $d = 16$ mm, (b) $d = 20$ mm.

that the peak displacement and peak output power of the three calculation models increase significantly, however, the interwell frequency bandwidth decreases.

Figures 4–6 show the steady-state amplitude response curves of the BPEH + TDM interwell motion displacement and output power with the variation of the base amplifier mass M_m for different stiffness ratios of k_f to k_b when excited frequency $\omega = 1.4$, $\omega = 1.7$, and $\omega = 2$. As can be seen from Figure 4, when excited frequency $\omega = 1.4$, the displacement amplitude and output power amplitude of the BPEH + TDM first increase to extreme values as the mass of the base amplifier M_m gradually increases, then rapidly decreases, and finally, tend to be stable in a small range, and there exists an optimal mass of the base amplifier mass M_m value which maximizes the displacement amplitude and output power amplitude of the system, and the optimal M_m value increases with the stiffness ratio of k_f to k_b increasing.

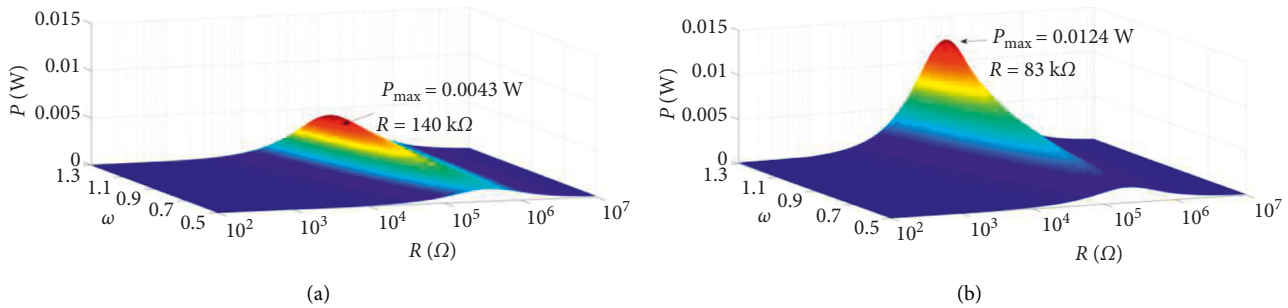

Figure 10: Output power amplitude response of the system with different load resistance: (a) $d = 18$ mm and (b) $d = 20$ mm.

Figures 5 and 6 show that when the excitation frequency increases, with the gradual increase of the M_m, the displacement amplitude and output power amplitude of the BPEH + TDM will first increase to the extreme value, then decreases sharply followed by a slight increase, and finally tend to be stable due to falling into the intrawell. It can also be seen from Figure 4 that with the increase of stiffness ratio k_f/k_b, the optimal value of M_m increases, and when M_m reaches the optimal value, the corresponding displacement amplitude and output power amplitude of the BPEH + TDM also increase with the stiffness ratio k_f/k_b increasing.

Figures 7–9 give the power amplitude variation curve with excited frequency for different values of the mass ratio M_f/M_t when $M_m = 0.12$ kg, $M_m = 0.15$ kg and $M_m = 0.18$ kg. Figures 7–9 show that when the base amplifier M_m and magnet spacing d are kept constant, the peak output power of the BPEH + TDM increases significantly as the mass ratio of the M_f to M_t increases and the excitation frequency at which the system generates peak power decreases. It can also be found from the results of Figures 7–9 that when magnet spacing d and mass ratio M_f/M_t remain unchanged, the peak output power of the BPEH + TDM decreases with the increase of M_m. However, the reduction rate of the peak power slows down as M_m becomes larger. When $d = 20$ mm, $M_f/M_t = 1.8$, taking $M_m = 0.15$ kg as examples, the peak power of the BPEH + TDM is 0.069 W, which is 21.6% lower than that of $M_m = 0.12$ kg. However, when M_m increases to 0.18 kg, the corresponding peak power of the BPEH + TDM is decreased by 14.3%, compared with that of $M_m = 0.15$ kg.

Figure 10 shows the variation of output power amplitude with load resistance for magnet spacing $d = 18$ mm and $d = 20$ mm. The results show the power amplitude tends to increase at the beginning and decrease afterwards with the increase of load resistance at each excited frequency. Each excitation frequency corresponds to an optimal load resistance to maximize the amplitude of power of the BPEH + TDM, and the optimal load resistance decreases with the increase of excitation frequency. The optimal resistance decreases with the increase of magnet spacing, but the corresponding peak power is significantly higher when the magnet spacing increases.

5. Conclusions

In this paper, based on the generalized Hamilton variational principle, considering the size effect and the rotary inertia of the tip magnet, an electro-mechanical coupling equation of the BPEH + TDM system is obtained, and the analytical solution of the equation is obtained by using the harmonic balance method. The effects of magnet spacing, the mass of the base dynamic magnifier M_m, the load resistance, the stiffness ratio of the k_f to k_b, and the mass ratio of the M_f to M_t on the BPEH + TDM system are investigated and the following conclusions were obtained:

(1) Increasing the magnet spacing can improve the interwell output power amplitude of the BPEH + TDM system, but the interwell frequency bandwidth decreases.

(2) There exists an optimal mass of the base dynamic magnifier to maximize the output power of the BPEH + TDM system, and the optimal value of the base dynamic magnifier mass increases with the increase of stiffness ratio k_f/k_b.

(3) The peak output power of the BPEH + TDM system increases significantly as the mass ratio of the M_f to M_t increases, and the excitation frequency at which the system generates peak power decreases with increasing M_f/M_t. The peak output power of the BPEH + TDM decreases with the increase of M_m. However, the reduction rate of the peak power slows down when M_m is large.

(4) Compared with the BPEH + DM1 system which a dynamic amplifier is placed between the fixed end of the piezoelectric beam and the BPEH + DM2 system which a dynamic amplifier is placed between the BPEH and the base structure, the BPEH + TDM system can produce higher peak output power and wider interwell bandwidth.

In many cases, the excitation of piezoelectric energy capture devices is mostly random. In the future, to further explore the strategy of inducing the multistable energy harvester to vibrate on the high energy orbit for low-level random excitation is of great significance to improve the application of piezoelectric energy harvesting.

Data Availability

The data used to support the findings of this study are available from the corresponding author upon request.

Conflicts of Interest

The authors declare that they have no conflicts of interest.

Acknowledgments

This research was funded by the Doctoral Startup Foundation of Anhui Jianzhu University (Grant no. 2020QDZ07), the Project of Science and Technology Plan of Department of Housing and Urban-Rural Development of Anhui Province (Grant no. 2020-YF15).

References

[1] M. Safaei, H. A. Sodano, and R. Anton, "A review of energy harvesting using piezoelectric materials: state-of-the-art a decade later," *Smart Materials and Structures*, vol. 28, no. 11, Article ID 113001, 2019.

[2] S. Zhou, M. Lallart, and A. Erturk, "Multistable vibration energy harvesters: principle, progress, and perspectives," *Journal of Sound and Vibration*, vol. 528, Article ID 116886, 2022.

[3] A. Erturk and D. J. Inman, *Piezoelectric Energy Harvesting*, John Wiley & Sons, 2011.

[4] A. Erturk and D. J. Inman, "An experimentally validated bimorph cantilever model for piezoelectric energy harvesting from base excitations," *Smart Materials and Structures*, vol. 18, no. 2, Article ID 025009, 2008.

[5] F. Qian, T.-B. Xu, and L. Zuo, "Design, optimization, modeling and testing of a piezoelectric footwear energy harvester," *Energy Conversion and Management*, vol. 171, pp. 1352–1364, 2018.

[6] X. D. Xie, A. Carpinteri, and Q. Wang, "A theoretical model for a piezoelectric energy harvester with a tapered shape," *Engineering Structures*, vol. 144, pp. 19–25, 2017.

[7] G. Miao, S. Fang, S. Wang, and S. Zhou, "A low-frequency rotational electromagnetic energy harvester using a magnetic plucking mechanism," *Applied Energy*, vol. 305, Article ID 117838, 2022.

[8] Z. Li, Y. Liu, P. Yin et al., "Constituting abrupt magnetic flux density change for power density improvement in electromagnetic energy harvesting," *International Journal of Mechanical Sciences*, vol. 198, Article ID 106363, 2021.

[9] C. Wei and X. Jing, "A comprehensive review on vibration energy harvesting: modelling and realization," *Renewable and Sustainable Energy Reviews*, vol. 74, pp. 1–18, 2017.

[10] H. Qing, S. Jeong, S. Y. Jeong, T. H. Sung, and H. H. Yoo, "Investigation of the energy harvesting performance of aLambda-shaped piezoelectric energy harvester using an analytical model validated experimentally," *Smart Materials and Structures*, vol. 30, no. 7, Article ID 75017, 2021.

[11] J. Jung, P. Kim, J.-I. Lee, and J. Seok, "Nonlinear dynamic and energetic characteristics of piezoelectric energy harvester with two rotatable external magnets," *International Journal of Mechanical Sciences*, vol. 92, pp. 206–222, 2015.

[12] A. H. Hosseinloo and K. Turitsyn, "Non-resonant energy harvesting via an adaptive bistable potential," *Smart Materials and Structures*, vol. 25, no. 1, pp. 15010–15018, 2015.

[13] Z. Fang, Y. Zhang, L. Xiang, H. Ding, and L. Chen, "Complexification-averaging analysis on a giant magnetostrictive harvester integrated with a nonlinear energy sink," *Journal of Vibration and Acoustics-Transactions of the ASME*, vol. 140, no. 2, Article ID 021009, 2017.

[14] Y. Peng, Z. Xu, M. Wang et al., "Investigation of frequency-up conversion effect on the performance improvement of stack-based piezoelectric generators," *Renewable Energy*, vol. 172, pp. 551–563, 2021.

[15] K. Fan, Q. Tan, Y. Zhang, S. Liu, M. Cai, and Y. Zhu, "A monostable piezoelectric energy harvester for broadband low-level excitations," *Applied Physics Letters*, vol. 112, no. 12, Article ID 123901, 2018.

[16] A. Kumar, S. F. Ali, and A. Arockiarajan, "Exploring the benefifits of an asymmetric monostable potential function in broadband vibration energy harvesting," *Applied Physics Letters*, vol. 112, no. 23, Article ID 123901, 2018.

[17] A. Erturk, J. Hoffmann, and D. J. Inman, "A piezomagnetoelastic structure for broadband vibration energy harvesting," *Applied Physics Letters*, vol. 94, no. 25, Article ID 254102, 2009.

[18] A. Erturk and D. J. Inman, "Broadband piezoelectric power generation on high-energy orbits of the bistable Duffing oscillator with electromechanical coupling," *Journal of Sound and Vibration*, vol. 330, no. 10, pp. 2339–2353, 2011.

[19] S. Fang, S. Zhou, D. Yurchenko, T. Yang, and W.-H. Liao, "Multistability phenomenon in signal processing, energy harvesting, composite structures, and metamaterials: a review," *Mechanical Systems and Signal Processing*, vol. 166, Article ID 108419, 2022.

[20] T. Yang and Q. Cao, "Dynamics and performance evaluation of a novel tristable hybrid energy harvester for ultra-low level vibration resources," *International Journal of Mechanical Sciences*, vol. 156, pp. 123–136, 2019.

[21] N. Tran, M. H. Ghayesh, and M. Arjomandi, "Ambient vibration energy harvesters: a review on nonlinear techniques for performance enhancement," *International Journal of Engineering Science*, vol. 127, pp. 162–185, 2018.

[22] R. L. Harne and K. W. Wang, "A review of the recent research on vibration energy harvesting via bistable systems," *Smart Materials and Structures*, vol. 22, no. 2, Article ID 023001, 2013.

[23] S. C. Stanton, C. C. McGehee, and B. P. Mann, "Nonlinear dynamics for broadband energy harvesting: investigation of a bistable piezoelectric inertial generator," *Physica D: Nonlinear Phenomena*, vol. 239, no. 10, pp. 640–653, 2010.

[24] S. C. Stanton, B. A. Owens, and B. P. Mann, "Harmonic balance analysis of the bistable piezoelectric inertial generator," *Journal of Sound and Vibration*, vol. 331, no. 15, pp. 3617–3627, 2015.

[25] Q. He and M. F. Daqaq, "Influence of potential function asymmetries on the performance of nonlinear energy harvesters under white noise," in *Proceedings of the International Design Engineering Technical Conferences and Computers and Information in Engineering Conference*, vol. 46391, Article ID V006T10A060, 2014.

[26] P. Kim, Y.-J. Yoon, and J. Seok, "Nonlinear dynamic analyses on a magnetopiezoelastic energy harvester with reversible hysteresis," *Nonlinear Dynamics*, vol. 83, no. 4, pp. 1823–1854, 2016.

[27] N. Yu, H. Ma, C. Wu, G. Yu, and B. Yan, "Modeling and experimental investigation of a novel bistable two-degree-of-freedom electromagnetic energy harvester," *Mechanical Systems and Signal Processing*, vol. 156, Article ID 107608, 2021.

[28] G. Sebald, H. Kuwano, D. Guyomar, and B. Ducharne, "Simulation of a Duffing's oscillator for broadband piezoelectric energy harvesting," *Smart Materials and Structures*, vol. 20, no. 7, pp. 75022–75038, 2011.

[29] G. Sebald, H. Kuwano, D. Guyomar, and B. Ducharne, "Experimental Duffing oscillator for broadband piezoelectric energy harvesting," *Smart Materials and Structures*, vol. 20, no. 10, pp. 102001–102010, 2011.

[30] H. Li, H. Ding, X. Jing, W. Qin, and L. Chen, "Improving the performance of a tri-stable energy harvester with a staircase-shaped potential well," *Mechanical Systems and Signal Processing*, vol. 159, Article ID 107805, 2021.

[31] X. Ma, H. Li, S. Zhou, Z. Yang, and G. Litak, "Characterizing nonlinear characteristics of asymmetric tristable energy harvesters," *Mechanical Systems and Signal Processing*, vol. 168, Article ID 108612, 2022.

[32] G. Wang, Y. Ju, W.-H. Liao, Z. Zhao, Y. Li, and J. Tan, "A hybrid piezoelectric device combining a tri-stable energy harvester with an elastic base for low-orbit vibration energy harvesting enhancement," *Smart Materials and Structures*, vol. 30, no. 7, Article ID 075028, 2021.

[33] L. Tang and J. Wang, "Size effect of tip mass on performance of cantilevered piezoelectric energy harvester with a dynamic magnifier," *Acta Mechanica*, vol. 228, no. 11, pp. 3997–4015, 2017.

[34] D. W. Man, D. H. Xu, X. C Kuang, X. F. Kang, Q. H. Xu, and Y. Zhang, "Analysis of Dynamic Characteristics of Tristable Piezoelectric Energy Harvester Based on the Modified Model," *Mathematical Problems in Engineering*, 2021.

[35] D. Man, H. Xu, G. Xu, D. Xu, L. Tang, and Q. Xu, "Dynamic characteristics analysis of tri-stable cantilever piezoelectric energy harvester with a novel-type dynamic amplifier," *International Journal of Heat and Technology*, vol. 40, no. 2, pp. 619–626, 2022.